Journal of Materials Science: Materials in Electronics
https://doi.org/10.1007/s10854-018-9175-0

Chemically synthesized 3D nanostructured polypyrrole electrode for high performance supercapacitor applications

Anuradha B. Bhalerao[1] · Ravindra N. Bulakhe[2] · Prashant R. Deshmukh[2] · Jae-Jin Shim[2] · Keshav N. Nandurkar[3] · Bhiwa G. Wagh[1] · S. V. Prabhakar Vattikuti[4] · Chandrakant D. Lokhande[5]

Received: 7 October 2017 / Accepted: 23 April 2018

Abstract

Three-dimensional (3D) polypyrrole (Ppy) electrodes are directly grown on Ni foam using a solution-based cost effective chemical method and an in situ controlled precipitation route for supercapacitor application. The Ppy electrodes are characterized for their structural and morphological studies using X-ray diffraction (XRD), Fourier transform infrared (FT-IR) spectroscopy, scanning electron microscopy (SEM) and transmission electron microscopy. The XRD study revealed that Ppy electrodes are amorphous. SEM shows the formation of tiny spherical grains spread over the entire electrode surface. The FT-IR study confirms the formation of Ppy film on the electrode surface. The supercapacitive performance of the Ppy electrode using the cyclic voltammetry technique in a 3M KOH electrolyte shows a maximum specific capacitance of 931 F/g at a scan rate of 5 mV/s. Performance analysis of the supercapacitive electrode carried out using electrochemical impedance spectroscopy (EIS). A distorted semicircle in the high frequency region of EIS shows reduction in charge-transfer resistance.

1 Introduction

Supercapacitors have attracted immense attention for electrical energy storage systems because they offer higher power density than batteries and higher energy density than conventional capacitors. They not only drive electric vehicles but also provide back up for wind and solar energy [1–4]. Supercapacitors are divided into two types according to their energy storage mechanism; viz. (i) the electrical double layer capacitor (EDLC) that employs carbon as a large-surface-area electrode, and (ii) the pseudo-capacitor that utilizes metal oxide and conducting polymers as electrode materials [1, 5, 6].

Among the conducting polymers known today, Ppy has attracted attention because of a combination of high charge density (compared with carbon) and low cost (compared with metal oxides), along with good environmental stability [7–9]. It is stable in air and has favorable electrochemical properties, thermal stability, high conductivity, and outstanding mechanical properties [10, 11]. Potential technological applications of Ppy such as in electronic and electrochromic devices for corrosion protection, supercapacitors, sensors, batteries, and membrane separation have attracted immense attention from active research areas in polymer science and engineering in the recent years [12–19].

Pioneering work by many researchers report a variety of techniques to deposit Ppy-based supercapacitor electrodes. Yang et al. [20] prepared coaxial halloysite/Ppy tubular nanocomposites using chemical oxidative polymerization and reported a maximum specific capacitance of 522 F/g in 0.5M Na_2SO_4 electrolyte. An et al. [21] reported a specific capacitance of 433 F/g, for a Ppy/carbon composite prepared by chemical oxidation polymerization through ultrasound

Anuradha B. Bhalerao and Ravindra N. Bulakhe have contributed equally to this work.

✉ Anuradha B. Bhalerao
anuradhapawar@gmail.com

✉ Chandrakant D. Lokhande
l_chandrakant@yahoo.com

[1] Applied Science Department, K. K. Wagh Institute of Engineering Education and Research, Nasik 422 003, India

[2] School of Chemical Engineering, Yeungnam University, Gyeongsan, Gyeongbuk 712-749, Republic of Korea

[3] Department of Production Engineering, K. K. Wagh Institute of Engineering Education and Research, Nasik 422 003, India

[4] School of Mechanical Engineering, Yeungnam University, Gyeongsan, Gyeongbuk 712-749, Republic of Korea

[5] D. Y. Patil University, Kasaba Bawada, Kolhapur, M.S 416 006, India

Published online: 28 April 2018

irradiation. Sharma et al. [22] obtained a maximum specific capacitance of 400 F/g for thin films of pulse polymerized Ppy in acidic electrolyte. Galvanostatically prepared nanostructured Ppy had a specific capacitance of 400 F/g [4]. Zhang et al. studied the electrolyte effect and reported the maximum specific capacitance of 403 F/g in 1M H_2SO_4 electrolyte as compared to 281 F/g in 1M $NaNO_3$ electrolyte [23]. Fan and Maier obtained a porous nanostructured Ppy using an electrodeposition method with specific capacitance up to 480 F/g [24]. Zhao et al. synthesized Ppy nanowires under mild conditions with a specific capacitance of 420 F/g [25]. The techniques utilized by earlier researchers are costly and it is difficult to prepare large-scale polymer films with these techniques. Therefore, low-cost and facile methods remain to be explored [26]. Major research in Ppy electrode development is devoted to increasing energy density and power density. Simultaneous efforts have also been devoted to decreasing fabrication costs of Ppy electrodes. However, the specific capacitance offered by pure Ppy-based supercapacitor electrodes is in the range of 200–500 F/g [4, 20–24]. Hence, it is still challenging to achieve high capacitance Ppy-based supercapacitor electrodes with a cost-effective synthesis technique. Effective synthesis and exploitation of Ppy as a supercapacitive electrode to achieve high energy density and high power density has inspired tremendous research efforts.

In this investigation, we report a simple and inexpensive controlled chemical precipitation route for the deposition of Ppy electrodes on a three-dimensional (3D) conducting nickel foam (NF) substrate. The novelty of this work lies in the 3D nature of the Ppy electrodes. Further, a range of techniques are used to characterize these electrodes for structural and morphological study. The electrochemical characteristics of Ppy electrodes are evaluated using cyclic voltammetry (CV) and charge–discharge techniques. Electrochemical impedance spectroscopy (EIS) is carried out to examine carrier transport properties, determine equivalent circuit parameters, and analyze the performance of the supercapacitive electrode. The possible cause of the relatively high performance of the electrode is then discussed.

2 Materials and methods

2.1 Preparation of Ppy electrodes

Figure 1 shows a schematic of the controlled precipitation route for the deposition of the thin film of Ppy. This method offers two advantages: keeping costs low (as there is no need of a special instrument), and the ability to produce large area electrodes. The chemical bath was prepared by using A.R. grade 0.1M pyrrole [C_4H_5N], 0.1M ammonium persulfate (APS) [$(NH_4)_2S_2O_8$], and 0.1M oxalic acid [$C_2O_4H_2$], which

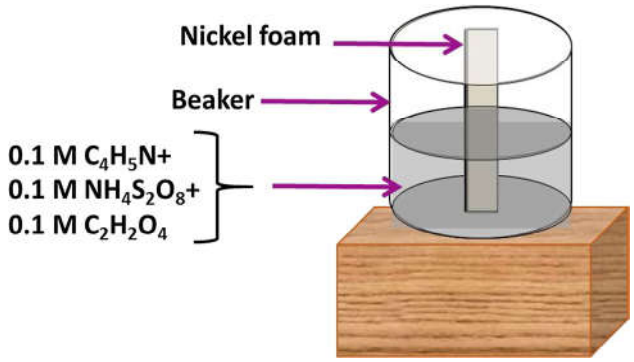

Fig. 1 Schematic of the controlled precipitation route for the deposition of the Ppy electrode

are separately dissolved in double distilled water. Here, APS acts as an oxidizing agent and oxalic acid functions as a reducing agent and chelating agent with the following dissociation reaction mechanism [27].

$$(NH_4)_2S_2O_8 \rightarrow 2NH_4^+ + S_2O_8^- + e^-$$

$$C_2O_4H_2 \rightarrow C_2O_4^{2-} + 2H^+$$

Pre-cleaning of 3D NF substrates (MTI Corporation, 1 cm × 3 cm × 1.6 mm thick) was carried out with 3M HCl solution under sonication for 15 min. followed by rinsing with deionized water and absolute ethanol. The pre-cleaned 3D NF substrates were vertically immersed in the bath [28]. The color of the bath gradually turned dark black indicating the polymerization of pyrrole at room temperature. A dark blackish Ppy electrode was formed on the substrate after 30 min. The NH_4^+ ion obtained from the dissociation of APS caused oxidation of the pyrrole by breaking a pi bond in the pyrrole, while $C_2O_4^{2-}$ ion [oxalate] from oxalic acid dissociation acts as stimulator for deprotonation and chelating agent to control reaction rate. The initiation reaction mechanism for the conversion of the pyrrole-to-pyrrole dimer is explained by Scheme 1. Pyrrole dimer formation is the primary step in the formation of polypyrrole [27].

2.2 Characterization techniques

The electrode material (Ppy) was structurally characterized by X-ray diffraction (XRD) and Fourier transform infrared (FT-IR) spectroscopy, and morphologically characterized by scanning electron microscopy (SEM) and transmission electron microscopy (TEM). XRD (PANalytical) was carried out using CuK (alpha) radiation. The morphology of the compounds was examined using a HITACHI, LTD S-4800 field emission scanning electron microscope. Morphology of the sample was confirmed by field emission transmission electron microscope (model CM 200) under

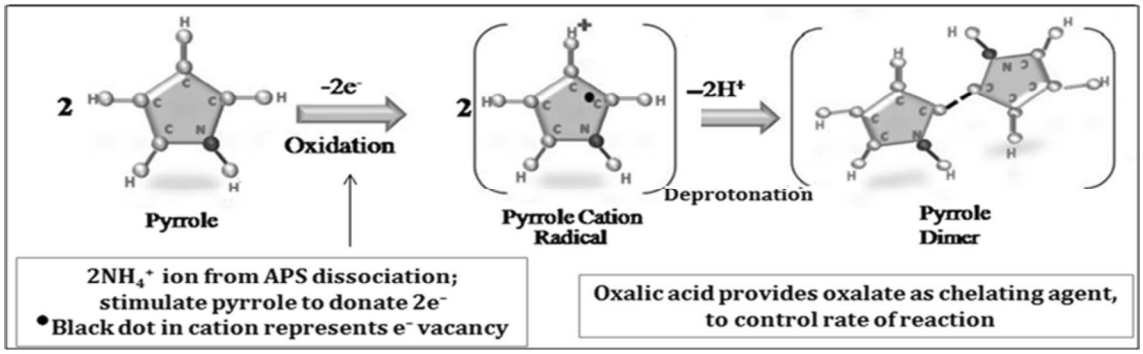

Scheme 1 Initiation mechanism showing conversion of pyrrole-to-pyrrole dimer [27]

scanning transmission electron microscopic imaging mode. The FT-IR spectrum was recorded in the spectral range of 450–4000 cm^{-1} using a Perkin Elmer spectrophotometer. The electrochemical measurements were carried out using a three-electrode configuration cell with a 3M KOH electrolyte. The nanohybrid electrodes (Ppy) on 3D NF were used directly as the working electrode, a platinum electrode as the counter, and a saturated calomel electrode (SCE) as the reference electrode. CV, galvanostatic charge–discharge cycling stability, and electrochemical impedance spectroscopic characterization was carried out to study the electrochemical performance of the prepared electrodes, using Auto Lab with Nova 1.10 software from the Netherlands [28].

3 Results and discussion

3.1 Structural study by XRD technique

The XRD pattern was recorded in the 2θ range 10–80°, with the intention of studying the crystalline nature of the Ppy electrode. The XRD pattern (Fig. 2) of the Ppy electrode shows three characteristic peaks at 2θ = 44.45°, 51.71°, and 76.41°. As per JCPDF data file 04-0850, these peaks are of phase-pure nickel metal substrate [29]. XRD pattern shows no diffraction peak i.e. non periodic arrangement of synthesized Ppy, which confirms the amorphous nature of synthesized material. Dubal et al. reported similar amorphous results with 20 nm-sized Ppy nanoplates deposited by the successive ionic layer adsorption and reaction (SILAR) method [30]. Palaniappan and Manisankar reported the formation of amorphous Ppy by a greener mechanochemical route [31].

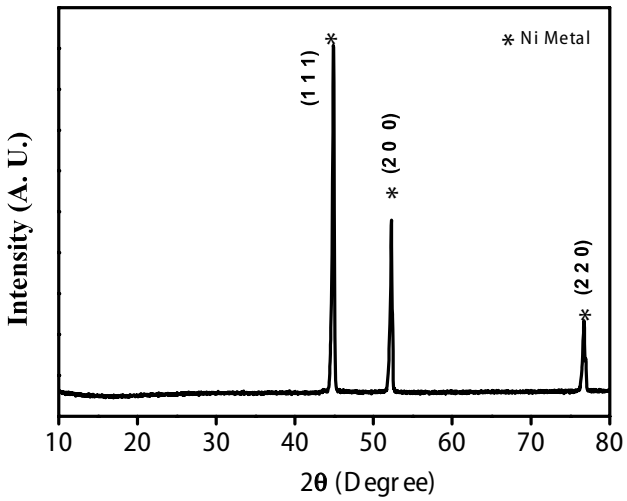

Fig. 2 XRD pattern of Ppy on the 3D NF substrate

3.2 Structural study by FT-IR spectrum analysis

The FT-IR spectrum of Ppy powder, scratched from NF, is shown in Fig. 3. The band observed at 3439 cm^{-1} was assigned to the –OH vibration band, which corresponds to

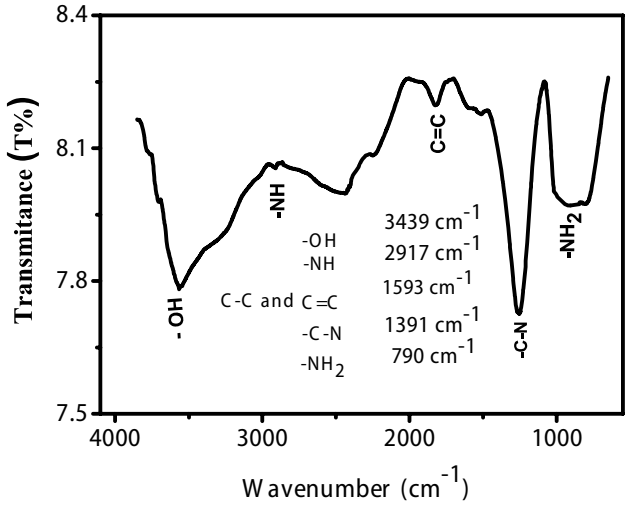

Fig. 3 FT-IR spectrum of Ppy

the presence of water molecules [32]. The peak at 2917 cm^{-1} corresponds to an N–H characteristic bond present in aromatic amines [33]. The absorption band at 1593 cm^{-1} was assigned to the pyrrole ring, i.e., the combination of C=C and C–C stretching vibrations [34]. The C–N stretching vibration was at around 1391 cm^{-1} [35]. The peak at 790 cm^{-1} was assigned to C=C in the plane bending of the pyrrole ring [36]. These characteristic bands confirm the formation of Ppy material.

FT-IR spectral analysis could also be interpreted by correlation with a physical explanation. During the chemical polymerization of pyrrole, electron neutrality was maintained by anions from the chemical bath. The free ion obtained from the oxidizing agent APS was combined with the pyrrole electron by breaking a pi bond in the pyrrole. The free electron in the pyrrole again combined with another pyrrole monomer to form a dimer pyrrole. Finally, a large number of such pyrrole dimer cations and radical cations combined to form a chain. Repeating the same process 'n' times, a long chain of Ppy was formed as shown in Scheme 2 [8, 37].

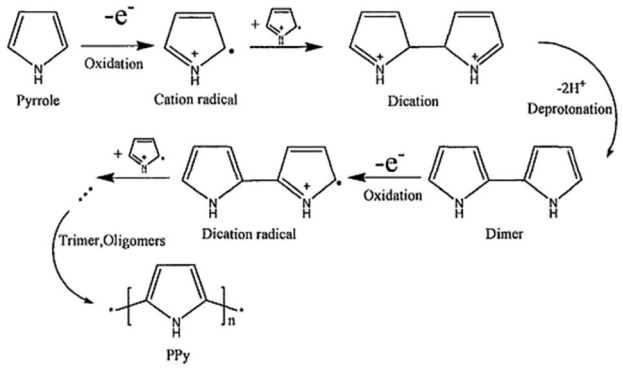

Scheme 2 Mechanism of chemical oxidative polymerization of Ppy

3.3 Surface morphology studies

The surface morphology of the Ppy electrode was studied by SEM. Figure 4 shows the SEM images of the Ppy electrode at different magnifications. Lower magnification image (50 µm, Fig. 4a) shows uniform coating and porous nature of Ppy on NF substrate. A porous electrode provides a higher surface area than its geometrical area. The high surface area

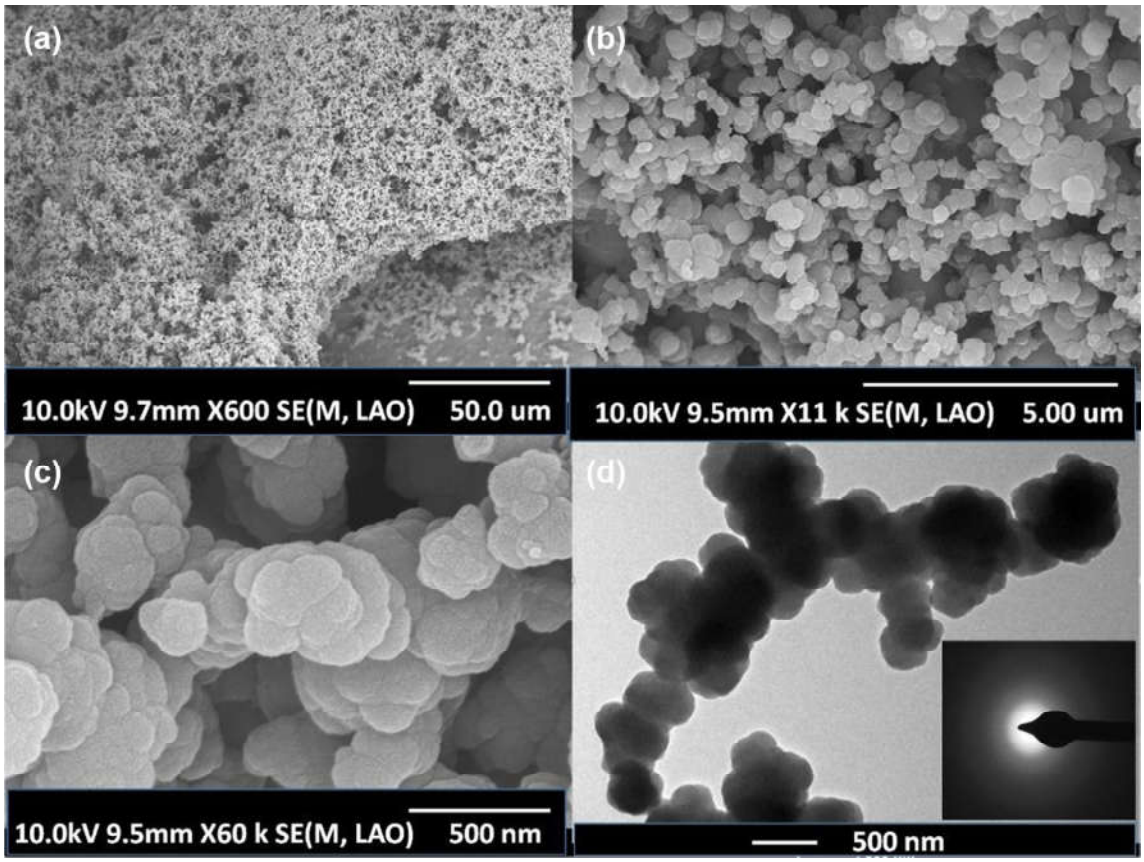

Fig. 4 Scanning electron micrographs of Ppy electrodes at different magnifications: (Fig. 4a, b and c). Transmission electron micrograph of Ppy electrode (Fig. 4d). Inset of Fig. 4d SAED pattern of Ppy

is useful for ion intercalation and deintercalation activity to provide enhanced electrochemical activity [38]. At higher magnification (5 µm, Fig. 4b), uniform distribution of spherical particles over the entire substrate surface was observed, and an even higher magnification (500 nm, Fig. 4c) image shows spherical particles staking on one another forming aggregation of nucleates. The average size of spherical particles is around ~500 nm. The detailed morphology of these spherical particles was studied using TEM (Fig. 4d), which clearly shows that the particles of Ppy were composed of nanosized grains with an average diameter of ~500 nm. The TEM image also confirmed the aggregation of cotton-boll like spherical particles to provide spherical morphology. The selected area electron diffraction (SAED) pattern (inset Fig. 4d) do not show existence of crystalline plane, as diffraction rings are not observed, hence this confirms nanostructured amorphous nature of the Ppy material [39]. The root cause of spherical morphology formation can be explained with the help of the general concept of morphology formation in conducting polymers (Ppy is a conducting polymer). Conducting polymers possess nanosized structures based on the concept of nucleates [40, 41]. During the oxidative polymerization of pyrrole; pyrrole dimers to tetramers are gradually produced to act as nucleates or initiation centers. Nucleates are adsorbed on NF substrate. A polymer chain starts growing on these centers. Morphology of the adsorbed Ppy depends upon nature of anionic oxidizing agent, concentration of reaction mixture and preparation methods [27]. Spherical morphology is the result of random aggregation of nucleates followed by polymer chain growth. Formation of tubular or rod like morphology is possible when reaction mixture is diluted or initial template object is provided during growth [41]. Hence, morphologically formation of nanosized structure of Ppy is possible, but non periodic lattice arrangement; as confirmed from SAED and XRD pattern shows amorphous nature. Amorphous nature of material allows protons to flow easily thorough bulk of the electrode to enhance the utility of whole electrode for energy storage [27].

3.4 Supercapacitor study

CV was performed in the potential range of −0.1 to + 0.55 V to evaluate the supercapacitive performance of the Ppy electrodes in 3M KOH electrolyte. Figure 5 shows the effect of scan rate variation on the CV behavior of the Ppy electrode. As the scan rate increased from 5 to 100 mV/s, the area under the curves increased (current increased), i.e. the Ppy material demonstrated an ideal supercapacitive nature. Figure 6 shows the variation of the scan rate with specific capacitance as a function of scan rate. The Ppy electrode showed a maximum specific capacitance of 931 F/g at a scan rate of 5 mV/s. As the scan rate increased from 5 to

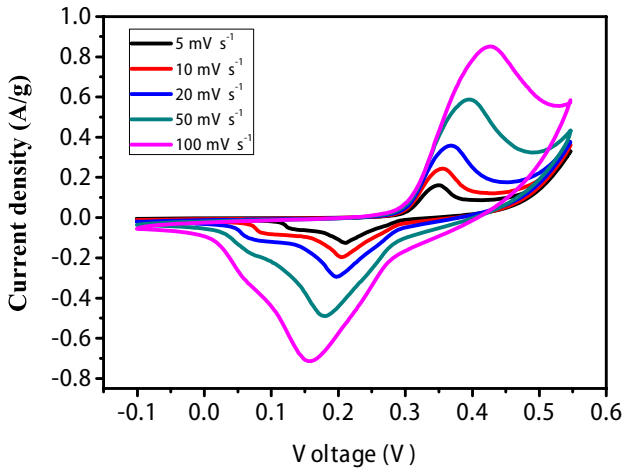

Fig. 5 Scan rate variation of Ppy measured in the potential range of −0.1 to + 0.55 V in 3M KOH electrolyte

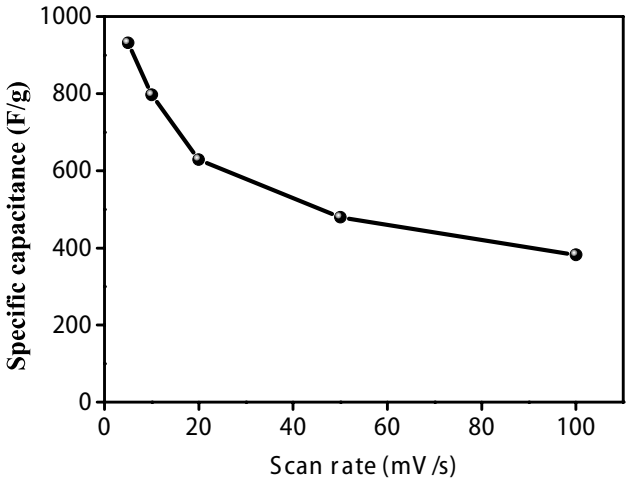

Fig. 6 Variation of scan rate (5–100 mV/s) verses specific capacitance of Ppy

100 mV/s, the specific capacitance values decreased from 931 to 640 F/g. Similarly, Shinde et al. [27] reported a maximum specific Ppy capacitance of 329 F/g by the chemical bath deposition (CBD) method. The decrease in capacitance was attributed to the presence of inner active sites that cannot sustain the redox transitions completely at higher scan rates. This was probably due to the diffusion effect of protons within the electrode. The decreasing trend of the capacitance suggests that parts of the surface of the electrode were inaccessible at high charging and discharging rates [42].

Figure 7 shows galvanostatic charge–discharge curves of the Ppy electrode measured in a 3M KOH electrolyte with current densities 2–8 A/g, in the potential window 0–0.4 V. The specific capacitance was calculated using the formula [43]:

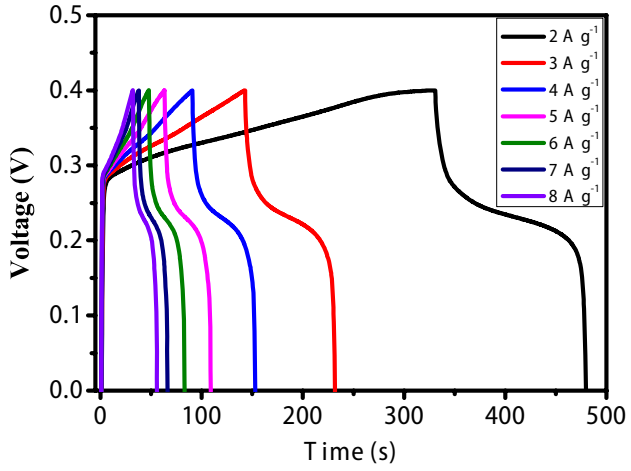

Fig. 7 Charge–discharge curves of Ppy electrode measured at 2, 3, 4, 5, 6, 7, and 8 A g^{-1} in the potential range of −0.1 to + 0.55 V in 3M KOH electrolyte

$$C_{cp} = \frac{I \times T_d}{V \times W}, \tag{1}$$

where I, T_d, V, and W denote current density, discharge time, potential range, and active weight of the electrode material, respectively. The voltage rise was instantaneous, whereas decay was exponential. Slow decay was attributed to the presence of surface states due to the porous nature of the material [44]. Figure 8 shows a plot of specific capacitances versus current densities at 2–8 A/g. The obtained maximum value of specific capacitance at current density 2 A/g was 923 F/g. The remarkable rise of specific capacitance reported in this study was the result of the 3D porous morphology of the Ppy electrode. It is clear from Fig. 8 that the data describes exponential decay curve. Specific capacitance decreases exponentially with increase in current density, indicating presence of faradaic oxidation and reduction reactions to transfer charge between electrode and electrolyte. Decrease in specific capacitance with increase in current density is due to decrease in involvement of active material in the redox reaction. At higher current densities, the actual surface area involved in redox process is insufficient, while at lower current densities interconnected Ppy particles participate in redox process [45]. In addition, there was an initial drop in potential caused by internal resistance. The energy density (E.D.) and power density (P.D.) are calculated, respectively, by the following equations [45]:

$$E.D. = \frac{V \times I_d \times T_d}{W}, \tag{2}$$

$$P.D. = \frac{V \times I_d}{W}, \tag{3}$$

where 'I_d' is discharge current, 'T_d' is the discharge time, 'V' is potential window, and W is the mass of the active material within the electrode i.e. the loaded mass of the Ppy electrode (0.510 mg). Figure 9 shows a Ragone plot of power density versus energy density. The power density varies from 0.9 to 3.7 kW/kg as the energy density varies from 26 to 37.5 Wh/kg respectively.

3.5 Ragone plot

The energy and power densities were determined, so as to determine the energy storage capability of the supercapacitor electrode. The Ragone plot was prepared using energy density versus power density for the Ppy electrode shown

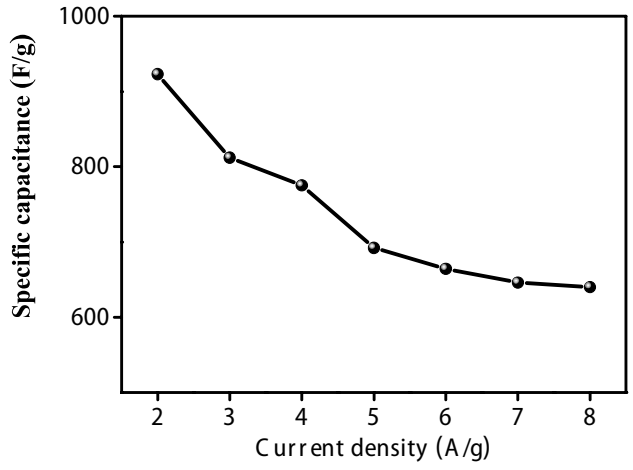

Fig. 8 Variation of current densities (2, 3, 4, 5, 6, 7, and 8 A/g) versus specific capacitance of Ppy electrode

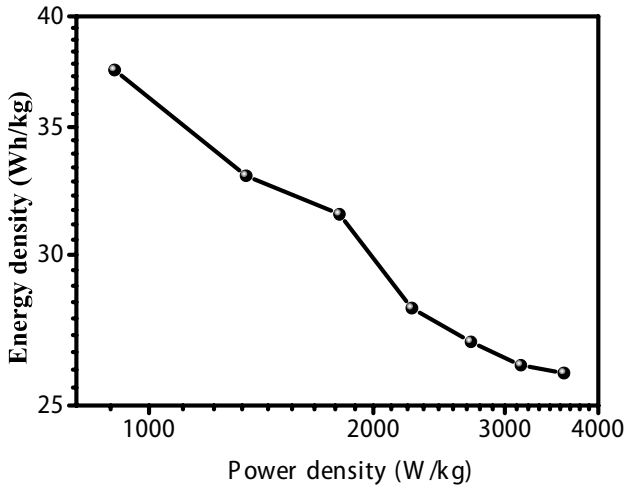

Fig. 9 Ragone plot of power density verses energy density of Ppy electrodes

in Fig. 9 at different current densities. The energy density of the Ppy electrode varied from 37.5 to 26 Wh/kg for current density increasing from 2 to 8 A/g. The Ppy electrode exhibited its maximum energy density of 37.5 Wh/kg at a power density of 0.9 kW/kg [46].

3.6 Stability study

Stability is one of the most important parameters in electrochemical study. Before the use of a chemically stable compound in any long-term application, it is necessary to check the stability of the electrode. A test of the cyclic stability of the Ppy electrode was carried out at the scan rate of 100 mV/s for the 1st to 5000th cycles. Figure 10 illustrates the variation of the cycle number with the specific capacitance of the Ppy electrode. The Ppy electrode exhibited 89% cyclic stability over 5000 cycles. The value of specific capacitance decreased from 640 to 576 F/g as cycles increased from 1 to 5000. The specific capacitance decreased due to the loss of active material caused by dissolution and/or detachment, during the early charging/discharging cycles in the electrolyte [43]. Dubal et al. reported that the cyclic stability for Ppy synthesized over 5000 cycles by electrodeposition methods and SILAR methods was 81 and 78%, respectively [31, 37]. Compared to SILAR and electrodeposition methods, the controlled precipitation route provides better stability for the Ppy electrode.

3.7 Electrochemical impedance study (EIS)

Figure 11 shows a Nyquist plot of a Ppy electrode obtained in 3 M KOH electrolyte, over a frequency range of 0.1 Hz to 40 kHz. An intercept at the high frequency region with the real part (Z′) was attributable to the combinational resistance (R_1), whereas the distorted semicircle was attributable to the

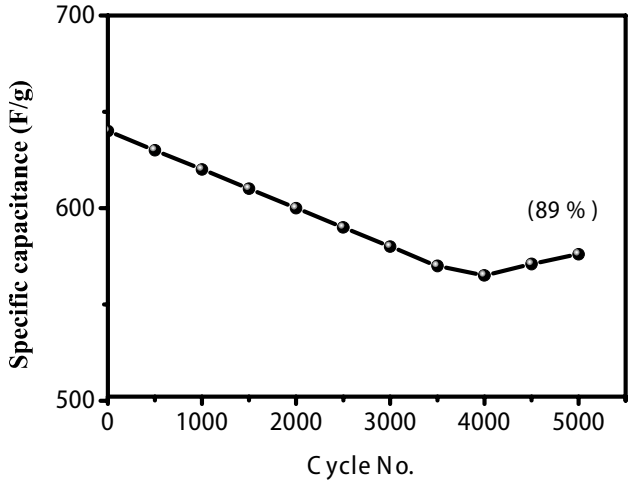

Fig. 10 Stability of the Ppy electrode over 5000 cycles

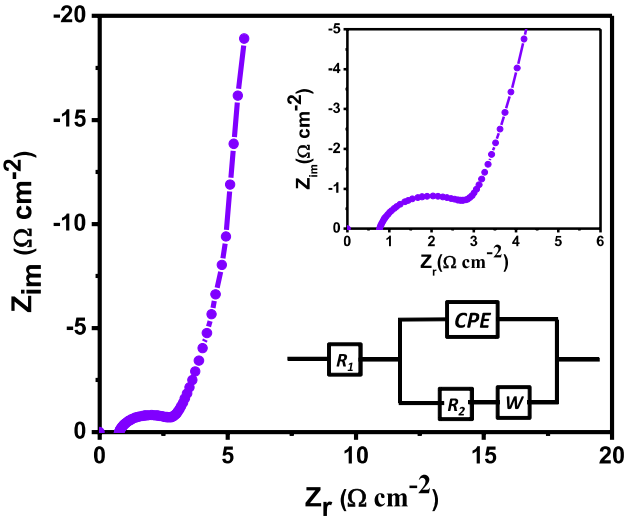

Fig. 11 Nyquist plot for Ppy, inset Fig. shows the distorted semicircle in the high frequency region and equivalent circuit for the fitted curve

charge transfer process at the composite electrolyte interface. The total resistance was found to be 0.8240 Ω, comprising the ionic resistance of the electrolyte, intrinsic resistance of the active material, and contact resistance of the active material and current collector [47]. A distorted semicircle was observed in the high frequency region. It resulted from a parallel combination of the charge-transfer resistance (R_2 = 1.29 Ω) and the constant phase element (CPE), and arose because of inhomogeneity in the electrode surface due to the random distribution of nanograins [48]. Zhao et al. reported a charge transfer resistance of 7.8 Ω for a Ppy electrode [25]. A comparison of charge transfer resistance with this recently reported value showed an enormous decrease in R_2 due to the 3D structure of Ppy. Reduced charge transfer resistance gave rise to new redox processes at the Ppy electrode/electrolyte interface. This caused hasty electron injection and electron drift [49]. The distorted semicircle is shown in the inset of Fig. 11. The impedance of CPE is given by:

$$Z(\omega) = Q^{-1}(j * \omega)^{-n} \quad (4)$$

The modulated parameters Q and n were equal to 0.00008309 $S{\cdot}s^n$ and 0.99041, respectively. At low frequency, the slope of a curve, closer to 35° with Z′, appeared; this may be related to the diffusion of counter ions between the electrolyte and electrode material. This is represented by the Warburg element (W), and the impedance is given by Zω. The diffusion coefficient (Aω) is fitted to be 16.511 $\Omega\ s^{-0.5}$ [50]. The Bode plots for Ppy are shown in Fig. 12. The total impedance of the electrode material increased with a decrease in frequency. The two humps in the Fig. were observed for phase angle variation; the one at around 21.54 Hz corresponded to a parallel combination of

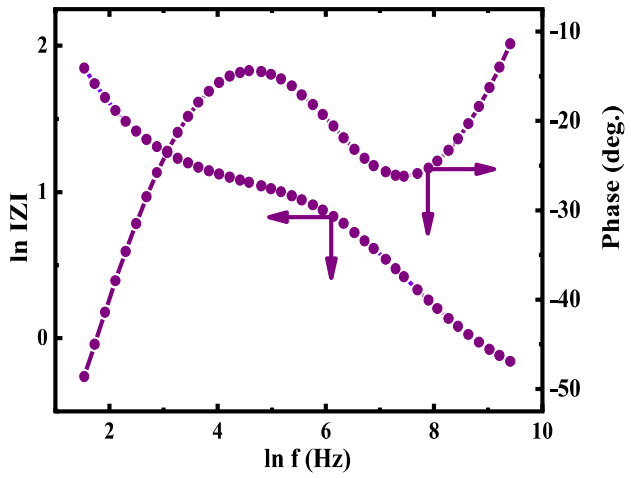

Fig. 12 Bode plots for Ppy, measured at an ac amplitude of 5 mV

CPE and R_2, whereas the other, at around 683.6 Hz, was due to the Warburg impedance (W). An equivalent circuit for a fitted curve is shown as an inset of Fig. 11.

4 Conclusions

In conclusion, 3D Ppy electrodes have been successfully synthesized by a cost effective and simple controlled chemical precipitation route at room temperature on a conducting 3D NF substrate. The Ppy was amorphous, and consisted of spherical particles with an average size of ~500 nm. The formation of Ppy material on the NF surface was confirmed by an FT-IR study. An electrochemical test shows that Ppy has good electrochemical performance, presenting a maximum specific capacitance of 931 F/g with high energy and power densities of 75 Wh/kg and 7.2 kW/kg, respectively. Ppy showed a good capacitance retention of 89% after 5000 cycles. The reduced charge transfer resistance is one of the reasons to enhance specific capacitance, making 3D Ppy a promising candidate for energy storage devices.

Acknowledgements The Priority Research Centers Program supported this research through the National Research Foundation of Korea (NRF), funded by the Ministry of Education (2014R1A6A1031189). In addition, the Basic Science Research Program through the National Research Foundation of Korea (NRF) funded by the Ministry of Education (NRF-2015R1D1A1A09060292), and the National Research Foundation (NRF) of Korea supported the work, and it was funded by the Ministry of Science, ICT, and Future Planning (2017R1A2B1004860).

References

1. P. Simon, Y. Gogotsi, Nat. Mater. 7, 845 (2008)
2. M. Winter, R.J. Brodd, Chem. Rev. 104, 4245 (2004)
3. B.E. Conway, W.G. Pell, J. Solid State Electrochem. 7, 637 (2003)
4. J. Wang, Y. Xu, F. Yan, J. Zhu, J. Wang, J. Power Sources 196, 2373 (2011)
5. R.K. Sharma, A.C. Rastogi, S.B. Desu, Electrochim. Acta 53, 7690 (2008)
6. R. Kotz, M. Carlen, Electrochim. Acta 45, 2483 (2000)
7. M. Bleha, V. Kudela, E. Yu, G.A. Rosova, A.G. Polotskaya, G.K. Kozlov, Elyashevich Eur. Polym. J. 35, 613 (1999)
8. R. Ansari, E. J. Chem. 3, 186 (2006)
9. B. Muthulakshmi, D. Kalpana, S. Pitchumani, N.G. Renganathan, J. Power Sources 158, 1533 (2006)
10. A. Laforgue, P. Simon, C. Sarrazin, J.F. Fauvarque, J. Power Sources 142, 80 (1999)
11. H.C. Kang, K.E. Geckeler, Polymer 41, 6931 (2000)
12. M. Natalie, R. Rowley, J. Mortimer, Sci. Prog. 85, 243 (2002)
13. N. Attarzadeh, K. Raeissi, M.A. Golozar, Prog. Org. Coat. 63, 167 (2008)
14. M.D. Ingram, H. Staesche, K.S. Ryder, J. Power Sources 129, 107 (2004)
15. K.H. An, K.K. Jeon, J.K. Heo, S.C. Lim, D.J. Bae, Y.H. Lee, J. Electrochem. Soc. 149, A 1058 (2002)
16. S. Sabah, M. Aghamohammadi, N. Alizadeh, Sens. Actuators B 114, 489 (2005)
17. Q. Zhou, C.M. Li, J. Li, X. Cui, D. Gervasio, J. Phys. Chem. C 111, 11216 (2007)
18. A. Mirmohseni, W.E. Price, G.G. Wallace, H. Zhao, J. Intell. Mater. Syst. Struct. 4, 43 (1993)
19. M.A. Smit, A.L. Ocampo, M.A. Espinosa-Medina, P.J. Sebastian, J. Power Sources 124, 59 (2003)
20. C. Yang, P. Liu, Y. Zhao, Electrochim. Acta 55, 6857 (2010)
21. H. An, Y. Wang, X. Wang, L. Zheng, X. Wang, L. Yi, L. Bai, X. Zhang, J. Power Sources 195, 6964 (2010)
22. R.K. Sharma, A.C. Rastogi, S.B. Desu, Electrochem. Commun. 10, 268 (2008)
23. J. Zhang, L. Kong, H. Li, Y.C. Luo, L. Kang, J. Mater. Sci. 45, 1947 (2010)
24. L.Z. Fan., J. Maier, Electrochem. Commun. 8, 937 (2006)
25. J. Zhao, J. Wu, B. Li, W. Du, Q. Huang, M. Zheng, H. Xue, H. Pang, Prog. Nat. Sci. 26, 237 (2016)
26. Y.G. Wang, H.Q. Li, Y.Y. Xia, Adv. Mater. 18, 2619 (2006)
27. S.S. Shinde, G.S. Gund, V.S. Kumbhar, B.H. Patil, C.D. Lokhande, Eur. Polym. J. 49, 3734 (2013)
28. R.N. Bulakhe, S. Sahoo, T.T. Nguyen, C.D. Lokhande, C. Roh, Y.R. Lee, J.J. Shim, RSC Adv. 6, 14844 (2016)
29. J. Tientong, S. Garcia, C.R. Thurber, T.D. Golden, J. Nanotechnol. 2014, 193161–193162 (2014)
30. D.P. Dubal, S.V. Patil, A.D. Jagadale, C.D. Lokhande, J. Alloy. Compd. 509, 8183 (2011)
31. S.P. Palaniappan, P. Manisankar, Mater. Chem. Phys. 122, 15 (2010)
32. D.P. Dubal, S.H. Lee, J.G. Kim, W.B. Kim, C.D. Lokhande, J. Mater. Chem. 22(7), 3044 (2012)
33. Q. Ameer, S.B. Adeloju, Sens. Actuators B 106, 541 (2005)
34. A.J.F. Romero, J.J.L. Cascales, T.F. Otero, J. Phys. Chem. B 109, 21078 (2005)
35. X.T. Zhang, J. Zhang, W.H. Song, Z.F. Liu, J. Phys. Chem. B 110, 1158 (2006)
36. S.T. Selvan, Chem. Commun. 3, 351 (1998)
37. A. Malinauskas, Polymer 42, 3957 (2001)
38. A.B. Bhalerao, B.G. Wagh, R.N. Bulakhe, A.D. Jagadale, C.D. Lokhande, Adv. Sci. Lett. 22, 759 (2016)
39. X. Yuan, L. Li, Z. Ma, X. Yu, X. Wen, Z.-F. Ma, L. Zhang, D.P. Wilkinson, J. Zhang, Sci. Rep. 6, 20005 (2016)
40. J. Stejskal, I. Sapurina, M. Trchova, Prog. Polym. Sci. 35, 1420 (2010)

41. J. Kopecka, D. Kopecky, M. Vrnata, P. Fitl, J. Stejskal, M. Trchova, P. Bober, Z. Morakova, J. Prokes, I. Sapurina, RSC Adv. 4, 1551 (2014)
42. T.P. Gujar, W.Y. Kim, I. Puspitasari, K.D. Jung, O.S. Joo, Int. J. Electrochem. Sci. 2, 666 (2007)
43. R. Ramya, M.V. Sangaranarayanan, J. Chem. Sci. 120, 31 (2008)
44. A.B. Bhalerao, B.G. Wagh, N.M. Shinde, S.B. Jambure, C.D. Lokhande, Energy Procedia 54, 549 (2014)
45. P.R. Deshmukh, S.N. Pusawale, A.D. Jagadale, C.D. Lokhande, J. Mater. Sci. 47, 1546 (2012)
46. S.J. Patil, B.H. Patil, R.N. Bulakhe, C.D. Lokhande, RSC Adv. 4(99), 56341 (2014)
47. Y. Li, K. Huang, D. Zeng, S. Liu, Z. Yao, J. Solid State Electrochem. 14, 1205 (2010)
48. A. Bruke, J. Power Sources 91, 37 (2000)
49. A.B. Bhalerao, B.G. Wagh, R.N. Bulakhe, P.R. Deshmukh, J.J. Shim, C.D. Lokhande, J. Photochem. Photobiol. A 336, 69 (2017)
50. G.C. Silva, C.S. Fugivara, G. Tremiliosi Filho, P.T.A. Sumodjo, A.V. Benedetti, Electrochim. Acta 47, 1875 (2002)